remote sensing

MDPI

Article

Green Area Index and Soil Moisture Retrieval in Maize Fields Using Multi-Polarized C- and L-Band SAR Data and the Water Cloud Model

Jean Bouchat [1,*], Emma Tronquo [2], Anne Orban [3], Xavier Neyt [4], Niko E. C. Verhoest [2] and Pierre Defourny [1]

[1] Earth and Life Insitute, Université Catholique de Louvain, 1348 Louvain-la-Neuve, Belgium; pierre.defourny@uclouvain.be
[2] Hydro-Climate Extremes Lab, Ghent University, 9000 Ghent, Belgium; emma.tronquo@ugent.be (E.T.); niko.verhoest@ugent.be (N.E.C.V.)
[3] Centre Spatial de Liège, Université de Liège, 4031 Angleur, Belgium; aorban@uliege.be
[4] Signal and Image Centre, Royal Military Academy, 1000 Brussels, Belgium; xavier.neyt@rma.ac.be
* Correspondence: jean.bouchat@uclouvain.be

Abstract: The green area index (GAI) and the soil moisture under the canopy are two key variables for agricultural monitoring. The current most accurate GAI estimation methods exploit optical data and are rendered ineffective in the case of frequent cloud cover. Synthetic aperture radar (SAR) measurements could allow the remote estimation of both variables at the parcel level, on a large scale and regardless of clouds. In this study, several methods were implemented and tested for the simultaneous estimation of both variables using the water cloud model (WCM) and dual-polarized radar backscatter measurements. The methods were tested on the BELSAR-Campaign data set consisting of in-situ measurements of bio-geophysical variables of vegetation and soil in maize fields combined with multi-polarized C- and L-band SAR data from Sentinel-1 and BELSAR. Accurate GAI estimates were obtained using a random forest regressor for the inversion of a pair of WCMs calibrated using cross and vertical co-polarized SAR data in L- and C-band, with correlation coefficients of 0.79 and 0.65 and RMSEs of 0.77 $m^2\,m^{-2}$ and 0.98 $m^2\,m^{-2}$, respectively, between estimates and in-situ measurements. The WCM, however, proved inadequate for soil moisture monitoring in the conditions of the campaign. These promising results indicate that GAI retrieval in maize crops using only dual-polarized radar data could successfully substitute for estimates derived from optical data.

Keywords: GAI retrieval; soil moisture; maize; SAR; L-band; multi-polarization; agriculture

Citation: Bouchat, J.; Tronquo, E.; Orban, A.; Neyt, X.; Verhoest, N.E.C.; Defourny, P. Green Area Index and Soil Moisture Retrieval in Maize Fields Using Multi-Polarized C- and L-Band SAR Data and the Water Cloud Model. *Remote Sens.* **2022**, *14*, 2496. https://doi.org/10.3390/rs14102496

Academic Editors: Kim Calders, Bas van Wesemael, Trissevgeni Stavrakou, Dimitry van der Zande, Hans Lievens, Jean-Christophe Schyns and Joost Vandenabeele

Received: 15 April 2022
Accepted: 21 May 2022
Published: 23 May 2022

1. Introduction

Monitoring the growth, health, and performance of crops throughout the growing season is an important aspect of agricultural management at the farm, regional or even global scale. Two variables of great relevance for crop monitoring are the green area index (GAI) [1,2] and the surface soil moisture under the canopy. The GAI, i.e., half of the total area of green plant in the canopy per unit of horizontal ground surface area ($m^2\,m^{-2}$), can be regarded as an extension of the more common leaf area index (LAI) to all photosynthetically active elements of the canopy [3]. Field measurements of GAI and soil moisture are, however, often too cumbersome to be carried out at large scale, whereas remote sensing can provide timely, cost-effective, and possibly accurate estimation methods.

While optical remote sensing systems are the most well-established operational agricultural monitoring systems today and have been successfully used for GAI retrieval, e.g., [4–7], as well as for soil moisture, though less effectively, e.g., [8–12], they are frequently impeded by the presence of clouds obscuring the view of the sensors [13]. Unlike

the latter, synthetic aperture radars (SAR) are weather-independent, active sensors able to penetrate the vegetation as well as the soil underneath in order to extract valuable information on them thanks to the sensitivity of microwaves to the dielectric and geometric properties of the objects with which they interact [14].

The sensitivity of SAR to the GAI and surface soil moisture of maize fields has been investigated in numerous empirical studies. Jiao et al. [15] reported high correlation coefficients between SAR backscatter signatures and GAI in maize in X-, C-, and L-band from TerraSAR-X, RADARSAT-2, and ALOS/PALSAR, respectively, which are the most commonly used frequency bands for agriculture monitoring. The frequency band of the radar signal is in fact a determining factor in its sensitivity to both GAI and soil moisture, mainly because the penetration depth of the signal into the canopy largely depends on it. In maize, a saturation phenomenon tends to occur to backscatter in C-band for GAI values exceeding 3 [16] to 4 $m^2 m^{-2}$ [17]. The penetration depth of the radar signal is even more decisive for soil moisture monitoring. If it is too shallow, microwaves cannot reach and interact with the ground, rendering the soil contribution to the backscatter negligible and the signal insensitive to surface soil moisture [18]. In their study on the penetration capabilities of SAR signals in C- and L-band, El Hajj et al. [19] reported that L-band waves can penetrate a well-developed vegetation cover of wheat or grass, i.e., with a normalized difference vegetation index (NDVI) larger than 0.7, and reach the underlying ground, whereas C-band waves proved to be more limiting. Backscatter data in L-band is therefore expected to allow for the monitoring of both vegetation biophysical variables and soil moisture in maize fields further into the later stages of plant development than backscatter in X- or C-band. Besides soil and vegetation characteristics, the sensitivity to GAI and soil moisture is also dependent on the sensor incidence angle and polarization. At shallow incidence angles, the contribution of the soil is reduced [18] while the vegetation contribution to the signal is enhanced [20]. At steep incidence angles, the attenuation of the signal by the vegetation is diminished and the soil contribution to the backscatter increases [21]. Regarding the polarization of the signal, the potential of the dual-polarized C-band data from Sentinel-1, and especially the ratio of its two available polarizations, for maize monitoring through its GAI was highlighted in [21–23]. Meanwhile, multiple studies have demonstrated the suitability of multi-polarization C- [24,25] and L-band [26] data for soil moisture monitoring under vegetation cover.

The retrieval of the vegetation biophysical variables of crops as well as the surface soil moisture from under their canopy using radar data has been addressed with varying degrees of success since the eighties, e.g., [27–33] One of the more widely used approaches for the operational monitoring of crops was proposed by Attema and Ulaby [34]. It is based on modeling the canopy of the crop as a cloud of identical and randomly distributed water droplets held in place by the vegetation matter. This approach resulted in a semi-empirical model for the backscattering coefficient of vegetated surfaces, called the water cloud model (WCM), which has been successfully used in a number of studies for the retrieval of various vegetation biophysical variables, e.g., [35–37], and of the surface soil moisture in the presence of a crop, e.g., [38–43]. The WCM simulates the radar backscattering coefficient of crops as the incoherent sum of the scattering from the vegetation layer and the contribution from the underlying soil attenuated by the canopy. The contribution of the soil is mainly driven by the surface soil moisture and the surface roughness, which can in some cases be neglected if it does not vary during the observation period. The contribution of the vegetation depends on one to two canopy descriptors, e.g., the GAI, which can then be retrieved by the inversion of the model with radar data and ancillary information on the contribution of the soil, mainly through its surface moisture [44]. However, relying on in-situ measurements or estimates of the surface soil moisture to retrieve the GAI of a crop renders the use of the WCM for operational crop monitoring impractical, even at a moderately large scale. To circumvent this problem, a system formed by a pair WCMs calibrated using different polarizations can be solved to simultaneously retrieve the GAI and the surface soil moisture of crops, dispensing with the need for in-situ measurements

or estimates of the latter. The feasibility of this method was investigated for the retrieval of the GAI of maize crops from C-band data using multiple inversion strategies [45], as well as the estimation of the biomass and soil moisture in winter wheat fields [46] and the GAI in maize and soybean fields [47] from C- and L-band multi-polarized SAR data, and retrieval accuracies similar to those of methods based on optical remote sensing were reported.

This study leverages an innovative data set built in 2018 in Belgium during a measurement campaign called BELSAR-Campaign. The data consist of C- and L-band SAR data as well as concurrent field measurements of biogeophysical variables of the vegetation and underlying soil acquired in eight maize fields representative of the area. The aim of this study is to develop and assess the potential of a method based on the WCM for the retrieval of the GAI in maize crops, as well as, secondarily, the surface soil moisture under the canopy, with SAR and in-situ data from the BELSAR campaign. First, the sensitivity of L-band backscatter to the maize GAI, the surface soil moisture under the canopy, and the incidence angle of the SAR beam, is assessed by means of a regression analysis, as well as forward modeling of the WCM. Then, the ability of the WCM to allow the retrieval of one of the two aforementioned variables at a time, with knowledge of the other, is investigated for each available SAR frequency and polarization. Finally, an algorithm is implemented for the simultaneous retrieval of both GAI and volumetric surface soil moisture in maize crops using only multi-polarized backscatter data and the incidence angle of the SAR beam, and its results are compared to those obtained with ancillary data on GAI or soil moisture.

2. Data

2.1. Site Description

The BELSAR airborne and field campaign that yielded the data set used in this study took place during the 2018 growing season, between the end of May and mid-September, in the BELAIR HESBANIA test site, between Gembloux and Sint-Truiden, Belgium. The site, which is depicted in Figure 1, belongs to the global JECAM network. It corresponds to a typical landscape of intensive agriculture of the Hesbaye region. It is mostly covered by relatively large, homogeneous, flat fields with a uniform topsoil texture of silt loam.

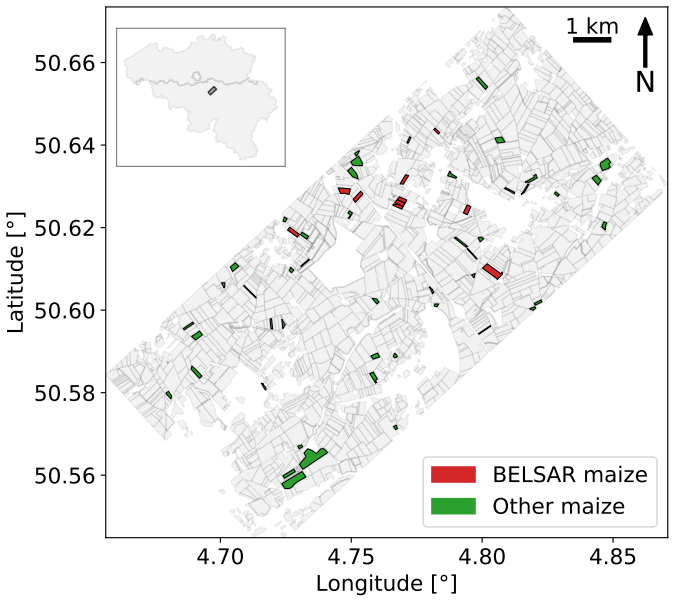

Figure 1. BELSAR area of interest, with the maize fields in which in-situ measurements were collected in red, the other maize fields in the area in green, and all the remaining agricultural fields inventoried as delineated in the Land Parcel Information System of Wallonia, Belgium, in grey.

2.2. SAR Data

2.2.1. L-Band from BELSAR

The L-band SAR data were collected from an airborne radar system operated by MetaSensing BV during the BELSAR campaign in a series of flights taking place approximately one month apart during the growing season of maize. Four radar acquisitions, named F1, F2, F3, and F4, coincided with the presence of maize crops in the imaged area, in Figure 1. Concurrent in-situ measurements of biogeophysical variables of crop and soil were recorded in eight maize fields following each of the flights. The dates of the airborne acquisitions and the corresponding in-situ measurements are reported in Table 1.

Table 1. Acquisition dates (day-month format) of the L- and C-band synthetic aperture radar (SAR) images from BELSAR and Sentinel-1, respectively, and of the corresponding in-situ measurements of vegetation and soil variables.

ID	SAR Measurements		In-Situ Measurements	
	BELSAR	**Sentinel-1**	**Vegetation**	**Soil**
F1	30-05	28-05	31-05 and 01-06	29-05
F2	20-06	21-06	21-06 and 22-06	20-06
F3	30-07	02-08	02-08	26-07
F4	28-08	26-08	29-08	28-08

The airborne L-band SAR system from MetaSensing BV [48] used in this study consisted of a left-looking sensor operating at a central frequency of 1.375 GHz and delivering fully polarimetric (HH, HV, VH, VV) radar images. The large available bandwidth of the system, up to 200 MHz, could not be exploited, however, due to constraints imposed by the Belgian Institute for Post and Telecommunications restricting it to 50 MHz. The cross-polarization channels, HV and VH, were averaged and the resulting channel was called HV to distinguish it from its C-band counterpart.

Radar data were processed by MetaSensing BV using the time-domain back-projection algorithm, performing motion compensation, and delivered as σ-calibrated single-look complex (SLC) focused SAR data. These radar images were co-registered based on the absolute position accuracy of the navigation data, i.e., around 0.75 m, and released in ground range geometry with a ground sampling distance of 1 m.

Four trihedral corner reflectors (CR) were deployed on site and used as standard point targets for the radiometric and polarimetric calibrations that were performed according to the procedure described in [49]. The radiometric calibration providing the σ^0 was based on the CR response and the calibration constant K was evaluated for each flight, F1 to F4. A polarimetric calibration was also applied in order to insure the images acquired in the different polarization channels correctly reflected the dependence of the target response to the polarization state of the signal. Data were calibrated for co-pol and cross-pol channel imbalances, that is, amplitude and relative phase differences between polarization channels, at both transmission and reception. Cross-talk was considered negligible, based on the obtained polarimetric signatures and CR impulse response function (IRF) showing sufficiently good isolation between the polarization at antenna level.

A 20 m inner buffer was applied to the boundaries of the fields in which in-situ data were collected to reduce border effects. Values of L-band backscattering coefficients σ^0 and incidence angle were then averaged over each of these fields. Their time series are represented in Figure 2.

A more in-depth description of the airborne L-band SAR data set from BELSAR can be found in [50].

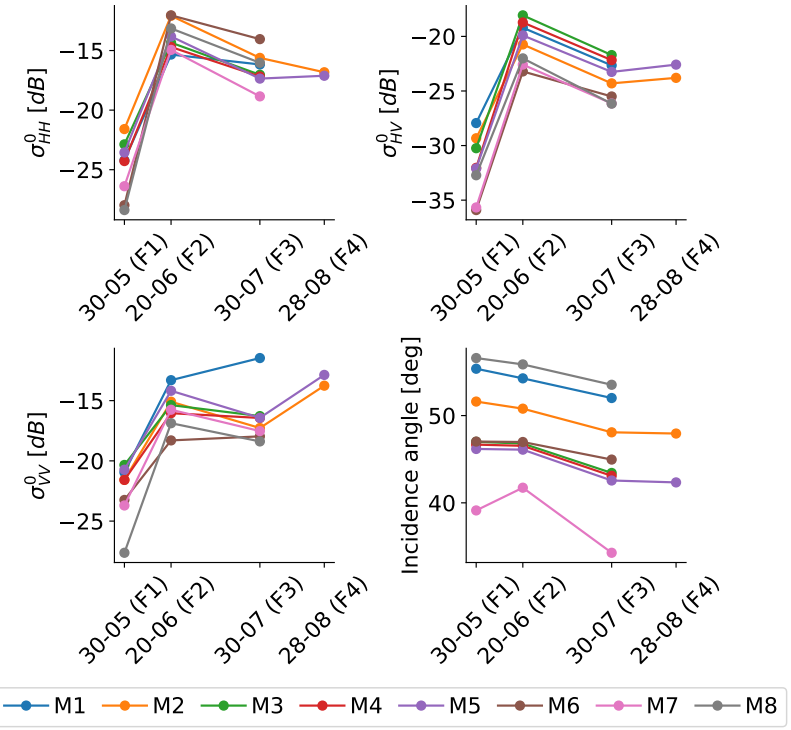

Figure 2. Time series of average L-band backscattering coefficient σ^0 and incidence angle acquired from an airplane during the BELSAR-Campaign. M1 to M8 designate the maize fields in which data were collected.

2.2.2. C-Band from Sentinel-1

Sentinel-1 is a constellation of two polar-orbiting satellites carrying SAR systems operating in C-band, at 5.405 GHz. The constellation, launched in 2014 and 2016, was designed and is operated by the European Space Agency (ESA) to provide radar imagery for the Copernicus program of the European Commission.

The study site in Figure 1 is imaged by the SAR systems of the Sentinel-1 constellation from four different orbits, numbered 37, 88, 110, and 161. Each orbit provides an image of the area of interest every 6 days in interferometric wide (IW) swath mode. However, in order to limit the effects of the morning dew and those resulting from modifications of the observation geometry, all the images used in this study were acquired from orbit 161. In this ascending orbit, the sensors pass over the area of interest at 5:32 p.m., with a mean incidence angle for the area of about 42°. The satellite images were acquired on 28 May, 21 June, 2 August and 26 August, with a maximum of 3 days of separation (mean 1.5 days) from the dates when in-situ measurements of biogeophysical variables were recorded in maize fields.

Sentinel-1 data were processed with ESA's Sentinel-1 toolbox (S1TBX) using the Sentinel Application Plateform (SNAP) [51]. The three main processing steps applied to the Level-1 SLC data in IW mode were, in order, the thermal noise removal, the radiometric calibration to obtain backscattering coefficients σ^0, and the range Doppler terrain correction using the Shuttle Radar Topography Mission (SRTM) 1 Arc-Second Global digital elevation model [52]. This procedure resulted in images of backscattering coefficients σ^0 and incidence angles with a 10 m ground sampling distance.

As with the L-band data, a 20 m inner buffer was applied to the fields in which in-situ data were collected and values of C-band backscattering coefficient σ^0 and incidence angle were then averaged over each of them. Their time series are represented in Figure 3.

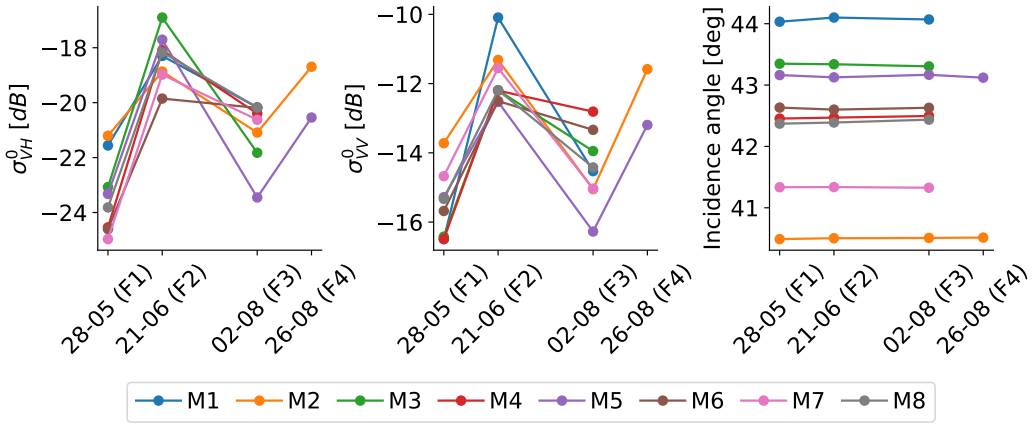

Figure 3. Time series of average C-band backscattering coefficient σ^0 and incidence angle from Sentinel-1 (orbit 161, ascending) imagery. M1 to M8 designate the maize fields in which data were collected.

2.3. In-Situ Measurements of Vegetation and Soil Variables

Synchronously with each airborne SAR acquisition, biogeophysical variables of vegetation and underlying soil were collected in eight maize fields in the imaged area, for a total of 26 data points. The fields are flat and homogeneous, with a surface area ranging from 1 to around 9 ha. Their location in the area of interest is depicted in Figure 1, and the correspondence between the acquisition dates of the radar images and the in-situ measurements can be found in Table 1.

Maize crop biophysical variables were collected in three representative plots inside each of the eight reference fields, and then averaged at the field level. These plots were selected according to their normalized difference vegetation index (NDVI), which had been computed from Pleiades images days prior to the start of the campaign. For each of the three plots in each reference field, green area index (GAI) measurements were derived from 10 digital hemispheric pictures, one every 3.75 m, with an approximate nadir view 1 m above the crop canopy, using the CAN-EYE software. The phenological development stage of the plants in each plot was also recorded. When first surveyed, on 31 May (F1), the maize plants were at the leaf-development stage, with five to eight leaves already unfolded. Then, on 21 June (F2), the plants were at the stem-elongation stage, with two to five nodes detectable. Next, on 2 August (F4), the crops were ripening and at their dough stage, with kernels yellowish at around 55% dry matter. Finally, on 28 August, only two fields remained unharvested and were fully ripe, with kernels hard and shiny at about 65% dry matter. These observations were described using the BBCH-scale [53]. A number of other maize biophysical variables were also collected during the BELSAR campaign [50]. They are partly reported in Table 2.

Volumetric soil moisture measurements were conducted using time domain reflectometry (TDR) sensors with 11 cm rods. At least 10 locations per reference field were monitored with three repetitions per location. All soil moisture measurements within each field were averaged to provide field average soil moisture values. The range of measured soil moisture values is 36 to 188 kg m^{-3}. In Belgium, such a low range depicts unusually dry conditions for the season. The summer of 2018 was indeed marked by an exceptional drought that accelerated the maturation of crops, which were consequently harvested several weeks earlier than usual.

Time series of the vegetation and soil biogeophysical variables collected in situ in the reference fields are represented in Figure 4.

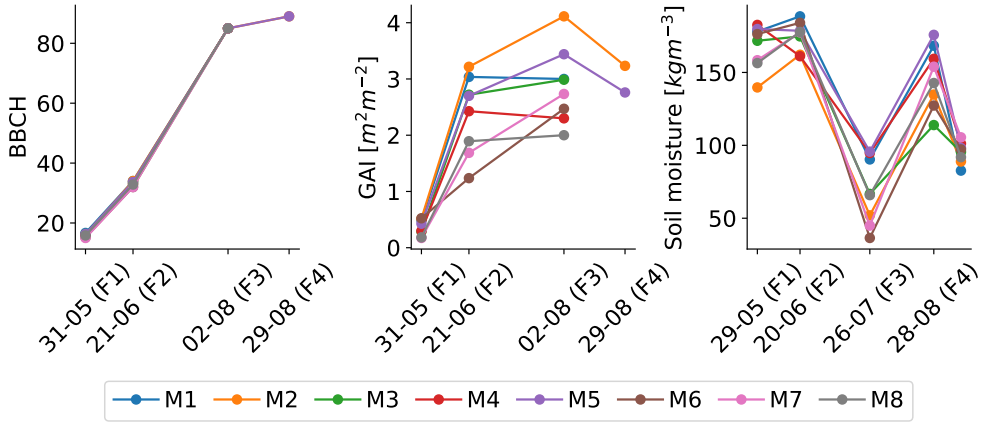

Figure 4. Time series of BBCH, volumetric surface soil moisture, and green area index (GAI) measured in situ in eight maize fields, M1 to M8, during the BELSAR-Campaign.

Table 2. Mean and standard deviation of several biophysical variables measured in the eight maize fields during the BELSAR campaign. Height and VWC designate the plant height and the vegetation water content. Dates are in the day-month format.

Date (ID)	BBCH		GAI [$m^2\,m^{-2}$]		Height [cm]		Biomass [$kg\,m^{-2}$]		VWC [$kg\,m^{-2}$]	
	Mean	Std	Mean	Std	Mean	Std	Mean	Std	Mean	Std
28-05 (F1)	15.8	0.6	0.4	0.1	40.4	8.2	0.2	0.1	0.2	0.1
21-06 (F2)	33.0	0.8	2.2	0.7	133.0	37.9	2.9	1.2	2.4	1.0
02-08 (F3)	85.0	0.0	2.8	0.6	245.3	33.9	5.2	0.9	3.8	0.7
26-08 (F4)	89.0	0.0	3.0	0.3	288.7	10.0	9.0	0.6	5.4	0.6

3. Methodology

3.1. SAR Signal Modeling

3.1.1. Water Cloud Model

Expressed in its current form by Prevot et al. [54], the water cloud model (WCM) is a semi-empirical model that simulates the backscattering coefficient of a vegetated field, σ^0_{tot}, in natural units, as the incoherent sum of the scattering from the vegetation, σ^0_{veg}, and the contribution from the underlying soil, σ^0_{soil}, attenuated by the canopy,

$$\sigma^0_{\text{tot}} = \sigma^0_{\text{veg}} + \tau^2 \sigma^0_{\text{soil}}. \tag{1}$$

The contribution of the vegetation is described as

$$\sigma^0_{\text{veg}} = AV_1 \cos(\theta)(1 - \tau^2), \tag{2}$$

where

$$\tau^2 = e^{-2BV_2 \sec(\theta)} \tag{3}$$

is the two-way attenuation through the canopy, θ is the incidence angle of the SAR signal beam, V_1, V_2 are vegetation descriptors, and A, B are model parameters. In this study, the vegetation descriptors, V_1 and V_2, are, respectively, 1 and the GAI ($m^2\,m^{-2}$) of the maize crop. The GAI is indeed a very suitable descriptor of the canopy since it is an indicator of light interception and thus, indirectly, photosynthesis [54]. As for the contribution from the soil to the backscatter, experimental evidence suggests that σ^0_{soil} in decibel (dB) is as a linear function of the volumetric surface soil moisture, V_m ($kg\,m^{-3}$) [55]. However, a closer fit was achieved with a linear relationship between σ^0_{soil} in natural units and V_m, hence,

$$\sigma^0_{\text{soil}} = CV_m - D, \tag{4}$$

where C and D are model parameters that account for the influence of soil moisture and soil roughness, respectively. This model implies that the soil roughness is constant throughout the observation period, i.e., the growing season of the crop, which is a reasonable assumption with respect to Belgian agricultural practices concerning maize.

3.1.2. Calibration

The model parameters A, B, C, and D were calibrated via non-linear least squares, which amounts to minimizing the sum of square residuals (SSR),

$$\min_{A,B,C,D} \sum_{i=0}^{N-1} (\sigma^0_{\text{obs},i} - \sigma^0_{\text{tot},i})^2, \tag{5}$$

where N is the number of data points in the calibration set, and $\sigma^0_{\text{obs},i}$ and $\sigma^0_{\text{tot},i}$, $i = 0, 1, \ldots, N-1$, are the backscattering coefficients, in natural units, observed and simulated with the WCM, respectively. This problem is solved numerically by alternating between the basin-hopping algorithm [56], which is a stepping technique for global optimization, and a truncated Newton method [57], for local minimization, starting from an initial guess (A_0, B_0, C_0, D_0) for the model parameters.

3.2. Backward Modeling

3.2.1. Algebraic Inversion

After the WCM is calibrated, it can be algebraically inverted in order to retrieve either the GAI or the volumetric surface soil moisture, V_m, of a maize crop. Hence, an estimate of the green area index,

$$\widehat{\text{GAI}} = -\frac{\cos(\theta)}{2B} \ln\left(\frac{A\cos(\theta) - \sigma^0_{\text{obs}}}{A\cos(\theta) - CV_m + D}\right), \tag{6}$$

and an estimate of the volumetric surface soil moisture,

$$\widehat{V_m} = \frac{1}{C}\left(\frac{\sigma^0_{\text{obs}} - A\cos(\theta)(1 - e^{-2B\,\text{GAI}\,\sec(\theta)})}{e^{-2B\,\text{GAI}\,\sec(\theta)}} + D\right), \tag{7}$$

can be obtained from a measurement of the backscattering coefficient, σ^0_{obs}, the incidence angle of the SAR signal beam, θ, and V_m or the GAI, respectively.

3.2.2. Simultaneous Retrieval of Green Area Index and Surface Soil Moisture

The algebraic inversion of the WCM allows to retrieve either the GAI or the surface soil moisture from SAR data with knowledge of the other variable. However, in-situ measurements of GAI and surface soil moisture are poorly suited to an operational setting. The use of two polarizations of a multi-polarized SAR measurement can dispense with the necessity to have knowledge of one of the two variables of interest, i.e., GAI and surface soil moisture, to obtain the other. Two WCMs can be calibrated using backscattering coefficients in different polarizations, forming a system of two non-linear equations with two unknowns, $\widehat{\text{GAI}}$ and $\widehat{V_m}$,

$$\begin{cases} \sigma^0_{\text{obs,pq}} = A_{\text{pq}}\,\widehat{\text{GAI}}\,\cos(\theta)\,(1 - e^{-2B_{\text{pq}}\sec(\theta)}) + (C_{\text{pq}}\widehat{V_m} - D_{\text{pq}})\,e^{-2B_{\text{pq}}\sec(\theta)} \\ \sigma^0_{\text{obs,rs}} = A_{\text{rs}}\,\widehat{\text{GAI}}\,\cos(\theta)\,(1 - e^{-2B_{\text{rs}}\sec(\theta)}) + (C_{\text{rs}}\widehat{V_m} - D_{\text{rs}})\,e^{-2B_{\text{rs}}\sec(\theta)} \end{cases} \tag{8}$$

where $\sigma^0_{\text{obs,pq}}$ and $\sigma^0_{\text{obs,rs}}$ are the measured backscattering coefficients in the pq and rs polarizations, and A_{pq}, B_{pq}, C_{pq}, D_{pq}, A_{rs}, B_{rs}, C_{rs}, D_{rs} are the parameters of the two WCMs, with $\text{pq}, \text{rs} \in \{\text{HH}, \text{HV}, \text{VV}\}$, $\text{pq} \neq \text{rs}$, for fully polarimetric data, and $\text{pq} = \text{VH}$, $\text{rs} = \text{VV}$ for dual-polarized data.

The resolution of (8) is an ill-posed problem. Several combinations of GAI and V_m can indeed correspond to a same SAR measurement [35]. Inversion techniques aim at

finding an approximate solution to the inverse problem by indirectly imposing additional constraints, which are dependent on their specific implementation, on the solution such that it becomes unique, thereby regularizing the problem. Three inversion techniques are explored and reported in this study: (1) an iterative optimization (IO) method [58]; (2) a look-up table (LUT) search; and (3) a random forest regressor (RFR) approach [59].

The IO method consists of finding solutions to (8) iteratively from an initial guess of the solution. The Levenberg–Marquardt algorithm [60] is used for this purpose. Since the existence of local minima cannot be excluded for the inverse problem, the method is not guaranteed to return the global minimum of the objective function. The possibility that its approximate solution is a local minimum depends largely on its initial approximation and its stopping criterion. In this paper, the latter specifies that the method stops when the approximate solution or objective value of the last iteration is too close to the ones of the previous iteration, or when a predetermined number of iterations is reached.

The LUT search begins by the generation of a data cube of simulated backscattering coefficients by forward modeling the pair of WCMs in (8) with varying values of GAI, V_m and θ. The inversion of a set of backscatter measurements and incidence angles is then performed by searching in the cube the entries that most closely correspond to them according to a criterion, the minimum Euclidean distance in this paper, and returning the GAI and soil moisture values from which they were simulated. In addition to the proximity criterion, the returned approximate solution therefore depends on the step size between the table entries and the criterion for choosing between multiple entries with identical proximity. In this study, if two inputs have the same distance to the observed radar data, the returned GAI and soil moisture values correspond to the entry for which their value as well as that of the incidence angle are the smallest.

Finally, the RFR consists in training a random forest on the data contained in the LUT to make up for the low amount of data observed in the field, and then using the trained model to produce estimates of the variables of interest from SAR measurements. The returned solution is computed as the mean of the predicted values of the variables of interest by the decision trees in the forest. As with the two previous inversion techniques, the choice of the hyperparameters, quantitative and categorical, of the method has an impact on the approximate solution that is found [61]. These hyperparameters can be the object of an optimization procedure, also called tuning, by various methods such as a grid search. The use of bootstrapping also introduces a random element in the method. It is therefore expected that the three inversion strategies listed above will produce different results between them and depending on the values of their hyperparameters. The comparison between these methods in this paper is therefore not absolute but relative to the problem presented and the experimental data collected.

3.3. Experimental Design

The main purpose of this study is to evaluate the performance of an algorithm based on the WCM for the simultaneous estimation of GAI and surface soil moisture in maize fields from radar data only. For this purpose, several methods, i.e., IO, LUT search, and RFR, are implemented and tested with the L- and C-band multi-polarized SAR, vegetation, and soil data from the BELSAR campaign. The results obtained are then compared to those that the WCM can deliver when one of the two variables of interest is known. A flowchart providing a summary of the different steps in the methodology of this study can be found in Figure 5.

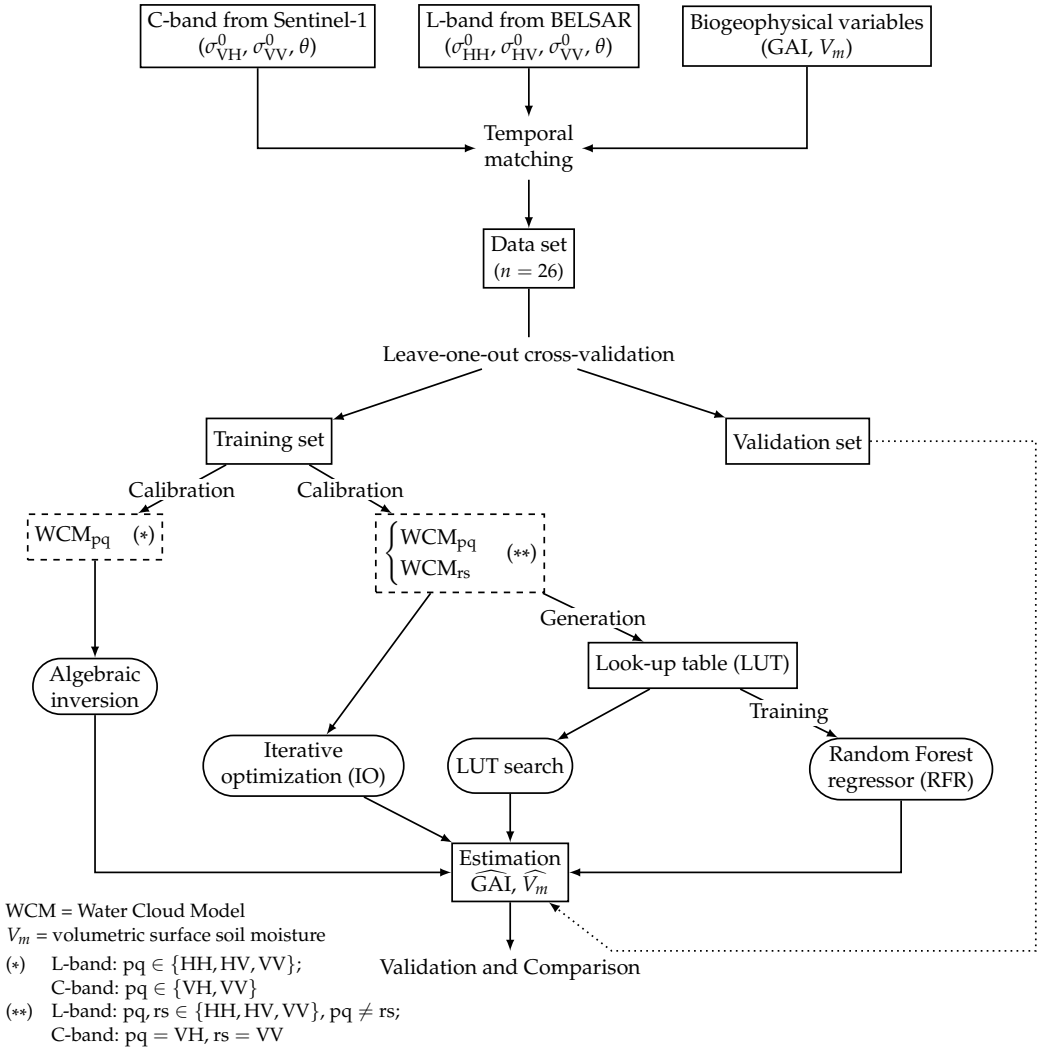

Figure 5. Flowchart of the experimental design.

3.4. Validation and Comparison between Inversion Methods

Since the amount of data that is available is relatively small, the goodness-of-fit and retrieval performance of the models are evaluated through a leave-one-out cross-validation (LOOCV) scheme. Let M be the number of data points in the data set. At each of the M iterations of the scheme, the model is trained on $M - 1$ data points. The remaining data point is then used to evaluate the goodness-of-fit of the WCM, by simulating the backscatter of the crop with the true values of the GAI, V_m, and θ of the data point, as well as the accuracy of the model predictions, by estimating the GAI and V_m from their corresponding radar measurements. The aggregation of these M evaluations through appropriate metrics then enables to evaluate the estimation performance of the different models and the ability of the WCM to simulate the backscatter of crops. The metrics used in this study to quantify the difference between estimated and observed values are Pearson's correlation coefficient, r, the root-mean-square error (RMSE), and the relative RMSE (rRMSE). The rRMSE is defined in this study as the RMSE divided by the difference between the maximum and minimum values of the observations. This normalization facilitates the comparison between data that has different ranges of values, such as the backscattering coefficients in co- and cross-polarization, as is apparent in Figures 2 and 3. For this reason, it is used in this study to evaluate the goodness-of-fit of the WCM, while the GAI and V_m estimates are evaluated with the RMSE to ease the comparison with state-of-the-art retrieval methods, as well as offer a more straightforward understanding of the real-world applicability of the investigated methods.

4. Results

4.1. Sensitivity Analysis

The potential of the C-band radar data from Sentinel-1 for maize monitoring has already been established and quantified in several studies, e.g., [21–23]. For this reason, only the sensitivity of the L-band backscatter measurements from the BELSAR data set to variations of the GAI, the volumetric surface soil moisture under the canopy, V_m, and incidence angle, θ, will be assessed in this study. This will be carried out in two ways. First using linear and linear-log regression models with the measured backscattering coefficients, as in [22,62]. Linear-log regression models are linear regression models computed using the logarithm of the independent variable. Second, by simulating backscattering coefficients with the WCM and observing their response to variations of GAI, V_m, and θ.

4.1.1. Sensitivity of L-Band σ^0 to GAI and V_m

The linear and linear-log regression lines, depicted in Figure 6, suggest through their coefficients of determinations, r^2_{lin} and $r^2_{lin\text{-}log}$, that the L-band backscattering coefficients σ^0 from BELSAR are moderately sensitive to the GAI, especially in HV, with $r^2_{lin} = 0.61$ and $r^2_{lin\text{-}log} = 0.73$, and in VV, with $r^2_{lin} = 0.63$ and $r^2_{lin\text{-}log} = 0.70$, but have no sensitivity to the surface soil moisture under the canopy, with $r^2_{lin} = 0.01$ and $r^2_{lin\text{-}log} = 0.01$ in HV, and $r^2_{lin} = 0.02$ and $r^2_{lin\text{-}log} = 0.01$ in VV. This finding is discussed in more detail by Bouchat et al. [50] in their study on the potential of the BELSAR airborne SAR acquisitions for agricultural applications, where the GAI is reported as the crop biophysical variable that is the most linearly correlated with the L-band backscattering coefficients used in this work, amongst all the crop variables measured in situ during the BELSAR campaign, i.e., GAI, plant height, wet and dry biomass, and vegetation water content which are reported in Table 2.

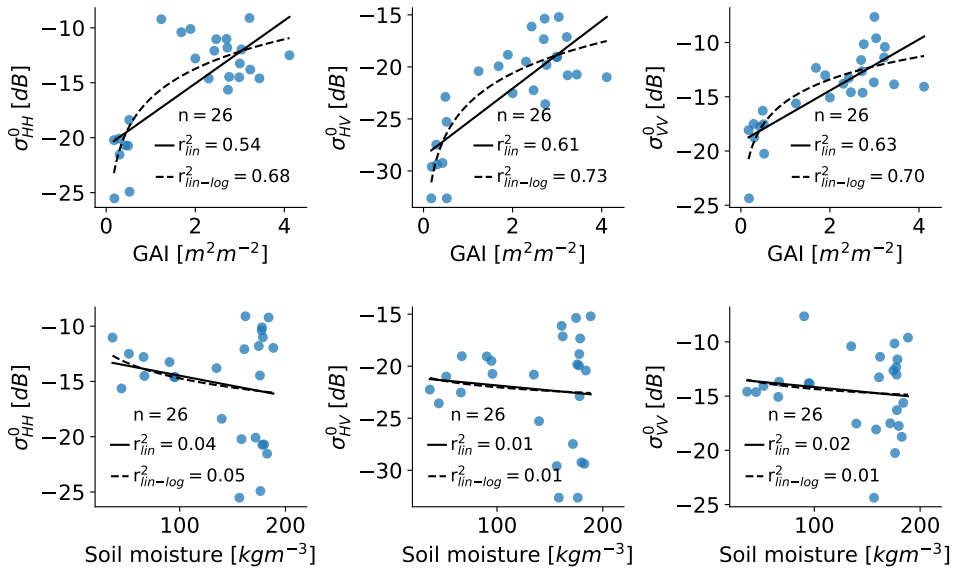

Figure 6. Scatter plots, as well as linear and linear-log regressions lines, of the volumetric surface soil moisture and GAI as a function of the backscattering coefficient σ^0 in HH, HV, and VV polarization.

4.1.2. Sensitivity of the Calibrated WCM to GAI, V_m, and θ

The sensitivity of the WCM, and of the L-band backscatter measurements through it, to variations of GAI, V_m, and θ is investigated by calibrating the WCM with the entire BELSAR data set ($n = 26$) for each polarization, and then forward modeling backscattering coefficients with varying values of the three variables on which it depends.

The values of the parameters of the WCM calibrated with HH, HV, and VV polarized L-band data from BELSAR are listed in Table 3. Note that the calibration procedure

for the WCM is based on the minimization of the sum of its squared residuals, a non-convex objective. While convergence to a global minimum cannot be guaranteed for this optimization problem, the minimization procedure, starting from an initial guess for values of the model parameters (A, B, C, and D), was found to be insensitive to this initial choice. Indeed, a range of initial values was tested for the start of the iterative minimization algorithm, and it was found that relatively large perturbations of these initial guesses have a negligible impact on the cross-validation errors made by the WCM. For this reason, all the calibration procedures of the WCM in this study have $(A_0, B_0, C_0, D_0) = (1, 1, 1, 1)$ as the initial guess.

Table 3. Values of the parameters of the water cloud model (WCM) calibrated with all available in-situ measurements of green area index (GAI) and volumetric surface soil moisture, V_m, and their corresponding L-band SAR backscattering coefficients and incidence angles.

Polarization	*A*	*B*	*C*	*D*
HH	1.35×10^{-1}	1.73×10^{-1}	7.88×10^{-4}	1.32×10^{-1}
HV	-3.24×10^{-2}	-6.58×10^{-2}	6.68×10^{-5}	9.74×10^{-3}
VV	-4.44×10^{-3}	-1.60×10^{-1}	7.48×10^{-5}	-4.58×10^{-3}

The fit of the WCM with the parameter values reported in Table 3 is similar in terms of RMSE for backscattering coefficients in HV and VV, with values of 0.16 and 0.15, respectively. However, the correlation coefficient in HV is higher than in VV, i.e., 0.83 against 0.72. The goodness-of-fit of the model is significantly worse in HH, with an r of 0.65 and an rRMSE of 0.22.

The backscattering coefficients simulations performed with the WCM calibrated with the parameter values listed in Table 3 for various values of GAI, V_m, and θ, are reported in Figures 7 and 8. These simulations provide insight on the sensitivity of the model, and indirectly the L-band SAR backscatter, to these variables. Variations in the value of the incidence angle have little overall effect on the sensitivity of the WCM simulations to variations in GAI or surface soil moisture values. Only the response of the model in VV is slightly affected by variations of θ, and only at high GAI values, i.e., around $4\,m^2\,m^{-2}$. Besides, the simulated backscattering coefficients in VV do not seem to converge, or saturate, with increasing GAI and are quite sensitive to variations in its value. On the other hand, they do not appear to be very sensitive to variations of the surface soil moisture value, V_m. The simulations in HV seem to be the most balanced, i.e., they are sensitive to changes in GAI and V_m, even at higher values, although this sensitivity decreases as GAI and V_m values increase. They are also more sensitive than those in VV to the surface soil moisture under the canopy. In general, the GAI has a significant impact on the sensitivity of the model to the surface soil moisture. This phenomenon is expected; the more developed the crop, the less capacity the signal has to penetrate it to interact with the soil. Finally, simulations in HH already saturate for moderately high values of GAI, at around $2\,m^2\,m^{-2}$, and are not very sensitive to soil moisture except at the early stages of crop growth.

Based on this sensitivity assessment, HV seems to be the most appropriate polarization for estimating GAI and V_m. It is then closely followed by VV, while HH appears insensitive to these biogeophysical variables in comparison.

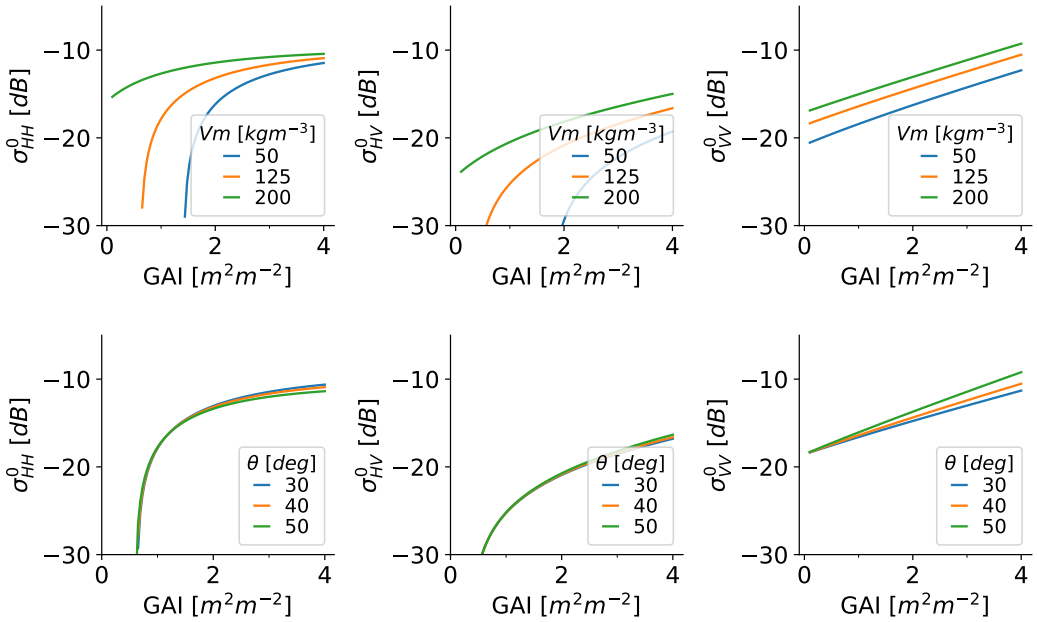

Figure 7. Backscattering coefficient simulations σ^0 in polarization HH, HV, and VV as a function of GAI (**top**) for multiple values of volumetric surface soil moisture, V_m, with the incidence angle $\theta = 40°$, and (**bottom**) for multiple incidence angles, with $V_m = 125\,\mathrm{kg\,m^{-3}}$.

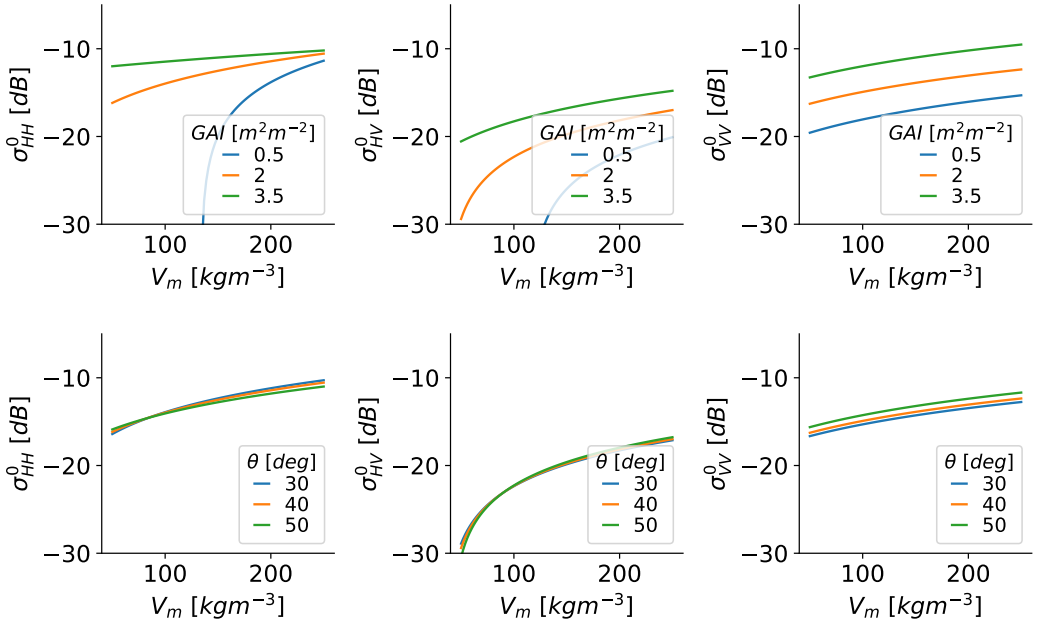

Figure 8. Backscattering coefficient simulations σ^0 in polarization HH, HV, and VV as a function of volumetric surface soil moisture, V_m, (**top**) for multiple values of GAI with the incidence angle $\theta = 40°$, and (**bottom**) for multiple incidence angles with GAI $= 2\,\mathrm{m^2\,m^{-2}}$.

4.2. Algebraic Inversion of the WCM

The retrieval of either the GAI or the volumetric surface soil moisture, V_m, is performed through the algebraic inversion of the WCM described in Section 3.2.1. This method requires the knowledge, or at least an estimate, of V_m to retrieve the GAI of a maize crop, and vice versa.

The quality of the fit between the measured backscattering coefficients and those simulated with the WCM, for each polarization, is depicted in Figures 9 and 10 for the L-band from BELSAR and C-band from Sentinel-1, respectively. The coefficients in the

figures are expressed in natural power units rather than decibels, even though the latter are more frequently encountered in the field of radar remote sensing. This is tied to the fact that the model is calibrated in these units and that the simulations of the semi-empirical model are not constrained in such way that they would have to be physically consistent, i.e., they can have negative values. This is indeed the case for the simulations in HH, in Figure 9a; therefore, the calibration results cannot be reported in decibels without omitting negative values.

In L-band, the fit of the simulations in HH, with a correlation coefficient of 0.47 and an rRMSE of 0.26, is significantly worse than for HV, with an r of 0.75 and an rRMSE of 0.18. In VV, the errors are highly influenced by only two data points that penalize the correlation coefficient and rRMSE, with values of 0.46 and 0.21, respectively. Without these outliers, given the tight distribution of the points along the 1:1 line, better results than in HV could be expected.

In C-band, despite errors in line with those obtained with L-band data, with correlation coefficients of 0.53 and 0.61, and rRMSEs of 0.21 and 0.22, for VH and VV, respectively, the model simulations appear to be less faithful to the backscattering coefficients measurements than those obtained with L-band data, as attested by the distribution of the data points in the scatter plots in Figure 10.

The estimates of GAI and V_m obtained through the algebraic inversion of the WCM, in a LOOCV scheme, are shown in Figure 11 for the L-band data, and in Figure 12 for the C-band data, and the estimation errors for each frequency band are reported in Table 4a and Table 4b, respectively.

The most accurate GAI estimates obtained using this method are derived from L-band SAR data in VV, with an r of 0.87 and an RMSE of 0.68 $m^2\,m^{-2}$. The vertical co-polarization, although leading to better GAI retrieval accuracies than HV, with an r of 0.85 and an RMSE of 0.75 $m^2\,m^{-2}$, is, on the other hand, less suitable than the latter for the estimation of the surface soil moisture, with an r of 0.60 and an RMSE of 54.73 $kg\,m^{-3}$ for HV, and an r of 0.39 and an RMSE of 81.25 $kg\,m^{-3}$ for VV. As for HH, its GAI and V_m retrieval accuracies are very low, with r values of 0.48 and 0.37 and RMSEs of 1.41 $m^2\,m^{-2}$ and 81.53 $kg\,m^{-3}$, respectively.

It is important to note, however, that threshold values were set to limit the values of the GAI estimates to a range between 0 and 4 $m^2\,m^{-2}$, as in [35], and V_m estimates between 0 and 250 $kg\,m^{-3}$. These extreme values used as prior information artificially increase the precision of the model estimates since they limit its least physically plausible outputs.

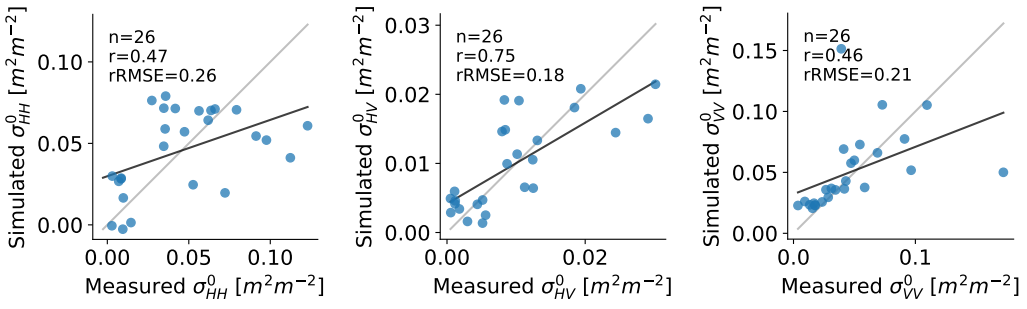

(**a**) HH (**b**) HV (**c**) VV

Figure 9. Results from the leave-one-out cross-validation (LOOCV) for the calibration of the water cloud model (WCM) with L-band data in (**a**) horizontal co-polarization, HH; (**b**) cross-polarization, HV; (**c**) vertical co-polarization, VV.

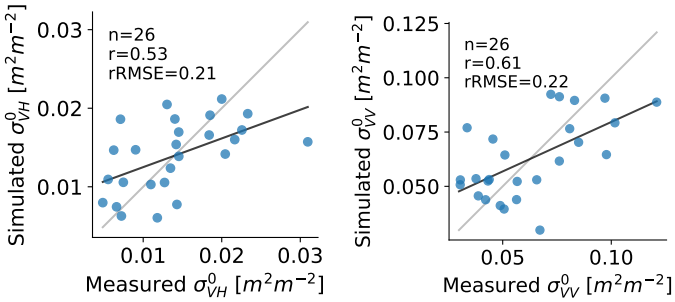

(**a**) VH (**b**) VV

Figure 10. Results from the LOOCV for the calibration of the WCM with C-band data in (**a**) cross-polarization, VH; (**b**) vertical co-polarization, VV.

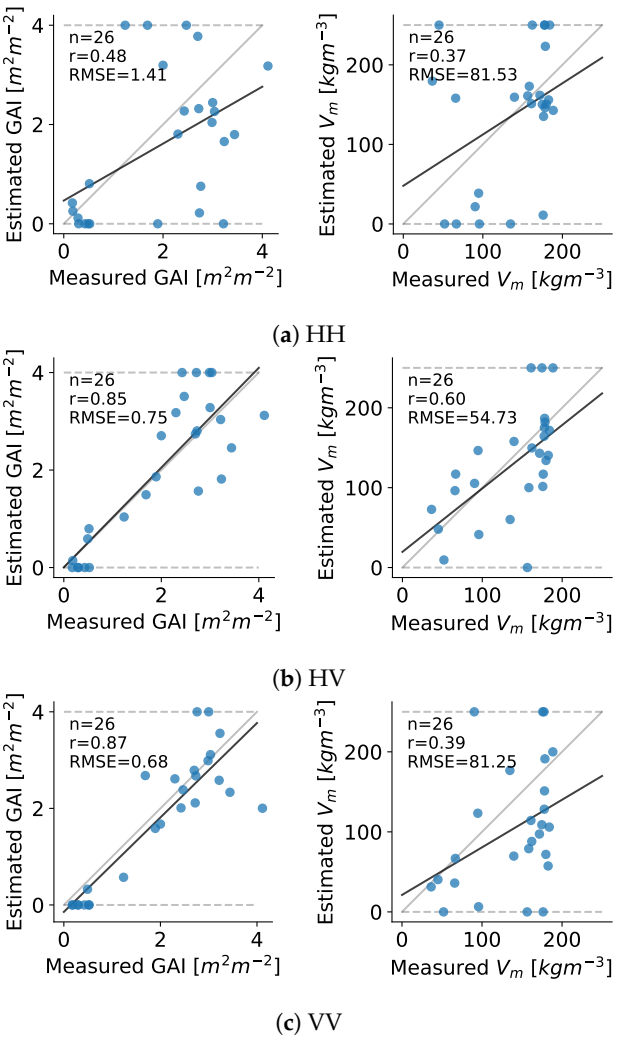

(**a**) HH

(**b**) HV

(**c**) VV

Figure 11. Results from the LOOCV for the retrieval of either maize GAI or volumetric surface soil moisture, V_m, using the algebraic inversion of the WCM with L-band data in (**a**) horizontal co-polarization, HH; (**b**) cross-polarization, HV; (**c**) vertical co-polarization, VV.

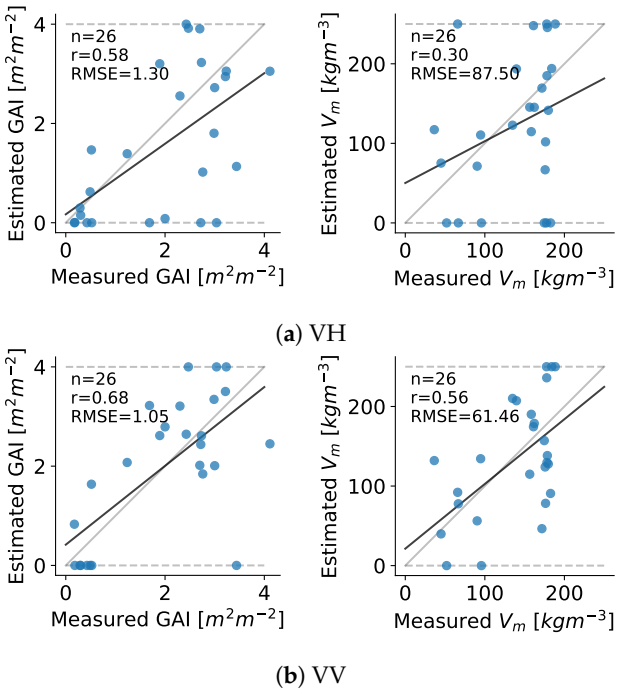

Figure 12. Results from the LOOCV for the retrieval of either maize GAI or volumetric surface soil moisture, V_m, using the algebraic inversion of the WCM with C-band data in (**a**) cross-polarization, VH; (**b**) vertical co-polarization, VV.

Table 4. Results from the leave-one-out cross-validation (LOOCV) for the retrieval of either GAI or volumetric surface soil moisture, V_m, in maize fields from (**a**) L- and (**b**) C-band backscattering measurements ($n = 26$) with the algebraic inversion of the WCM.

(a) L-Band				
Polarization	**GAI [$m^2\,m^{-2}$]**		**V_m [$kg\,m^{-3}$]**	
	r	**RMSE**	**r**	**RMSE**
HH	0.48	1.41	0.37	81.53
HV	0.85	0.75	0.60	54.73
VV	0.87	0.68	0.39	81.25
(b) C-Band				
Polarization	**GAI [$m^2\,m^{-2}$]**		**V_m [$kg\,m^{-3}$]**	
	r	**RMSE**	**r**	**RMSE**
VH	0.58	1.30	0.30	87.50
VV	0.68	1.05	0.56	61.46

4.3. Simultaneous Retrieval of Green Area Index and Surface Soil Moisture

The simultaneous retrieval of both GAI and V_m with dual-polarized SAR data (HH and HV, HH and VV, or HV and VV, for the L-band data, and VH and VV for the C-band data) is performed using three inversion strategies: the iterative optimization (IO) method, the look-up table (LUT) search, and the random forest regression (RFR). These are described in Section 3.2.2.

For the IO method, the initial values for the GAI and V_m required by the Levenberg–Marquardt algorithm were set at $2\,m^2\,m^{-2}$ and $125\,kg\,m^{-3}$. With regard to the LUT search and RFR, the pairs of backscattering coefficients forming the data cube were simulated from a grid of GAI, V_m, and θ values such that

$$\begin{aligned} \text{GAI} &= \{x : x = 0.05n,\ n \in \{0, 1, \ldots, 80\}\}, \\ V_m &= \{x : x = 0.5n,\ n \in \{0, 1, \ldots, 500\}\}, \\ \theta &= \{x : x = 20 + 0.5n,\ n \in \{0, 1, \ldots, 80\}\}. \end{aligned}$$

A grid search resulted in the number and maximum depth of the RFR trees being set at 100 and 4, respectively.

Since the WCMs are calibrated separately using distinct polarizations, the calibration results for this retrieval method are the same as the ones for the one relying on the algebraic inversion of the model. They are reported in Figures 9 and 10 for the L- and C-band data, respectively. As for the validation results from the LOOCV for each available frequency band and polarization pair, they are reported in Table 5.

In L-band, of the three inversion strategies, the RFR with the polarization pair HV and VV resulted in the most accurate estimates for both GAI and volumetric surface soil moisture, with an r of 0.79 and an RMSE of 0.77 $m^2\,m^{-2}$, and an r of 0.20 and an RMSE of 70.60 $kg\,m^{-3}$, respectively. These validation results, from the LOOCV with the RFR, as well those obtained with the other two polarization pairs, are depicted in Figure 13.

Of the three polarization pairs in this frequency band, the pair HV and VV provides the best GAI estimates for each inversion strategy. This finding does not hold for V_m, however, since the pair HH and HV yields a lower RMSE than the other pairs with the IO method, with a value of 80.75 $kg\,m^{-3}$, although these errors remain much larger than those obtained via the RFR. Furthermore, for each polarization pair, the GAI estimates obtained with the RFR are better than those of the other two inversion strategies, which is consistent with the findings of Mandal et al. [45] in their investigation into multiple inversion strategies for the estimation of the GAI in maize crops using the WCM with C-band data.

For the C-band data with the only available polarization pair, VH and VV, the strategy resulting in the most accurate GAI and V_m estimates is the RFR, as with the L-band, with correlation coefficients of 0.65 and 0.29, and RMSEs of 0.98 $m^2\,m^{-2}$ and 69.34 $kg\,m^{-3}$.

Based on these observations, the L-band seems, therefore, better suited for the estimation of the GAI with this method, and the C-band for the estimation of V_m, although results for the latter are quite close between the two frequency bands. However, this observation must be qualified. Concerning V_m, neither the estimates obtained from L-band data nor those obtained from C-band data seem to be usable for accurate soil moisture monitoring based on the loose distributions around the 1:1 line visible in Figures 13 and 14. As for the GAI, there is a clear overestimation of its value at the beginning of the growing season for both frequency bands. However, this may be due to an imbalance in the calibration data set.

Finally, this method, which consists of simultaneously estimating the GAI and volumetric surface soil moisture of a maize crop, thus provides similar, although slightly less accurate, results than the method based on the algebraic inversion of the WCM. However, the former has the decisive advantage, in an operational context, that it only requires backscattering measurements in two polarizations and the incidence angle of the SAR beam, and no ancillary information on either one of the variables of interest to provide estimates of the other. Note as well that for none of these strategies were the thresholds imposed for the estimates of GAI and V_m reached, unlike for the method based on the algebraic inversion of the WCM.

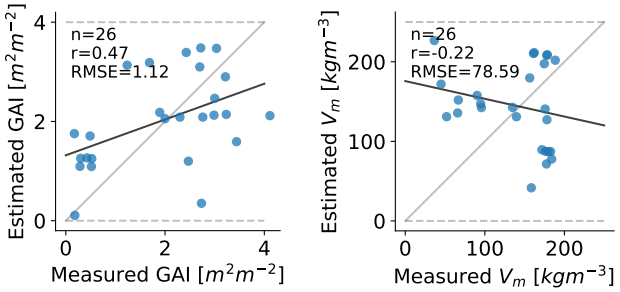

(**a**) HH and HV

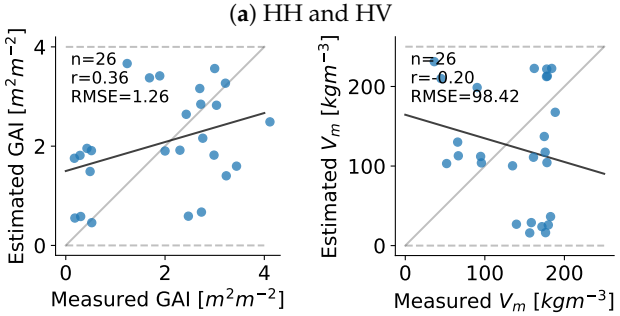

(**b**) HH and VV

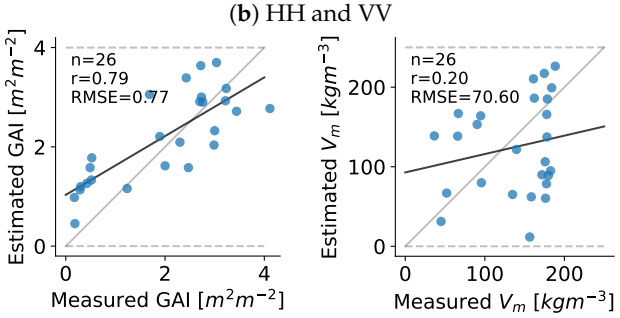

(**c**) HV and VV

Figure 13. Results from the LOOCV for the simultaneous retrieval of maize GAI and volumetric surface soil moisture, V_m, from (**a**) HH and HV; (**b**) HH and VV; (**c**) HV and VV polarization pairs, using a random forest regressor (RFR).

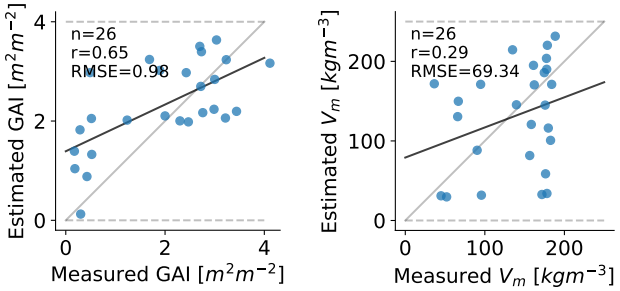

Figure 14. Results from the LOOCV for the simultaneous retrieval of maize GAI and volumetric surface soil moisture, V_m, using a RFR with C-band data in VH and VV polarizations.

Table 5. Results from the LOOCV for the simultaneous retrieval of GAI and volumetric surface soil moisture, V_m, in maize fields from (**a**) L- and (**b**) C-band backscattering measurements ($n = 26$) with different inversion strategies for the WCM: the iterative optimization method (IO), the look-up table search (LUT), and the random forest regressor (RFR).

(a) L-Band					
Method	**Polarizations**	**GAI [$m^2\,m^{-2}$]**		**V_m [$kg\,m^{-3}$]**	
		r	**RMSE**	**r**	**RMSE**
IO	HH and HV	0.32	1.46	0.21	80.75
	HH and VV	0.17	1.49	−0.36	127.28
	HV and VV	0.69	1.16	0.28	92.43
LUT	HH and HV	0.10	1.60	−0.25	89.65
	HH and VV	0.43	1.26	−0.30	118.16
	HV and VV	0.76	1.00	0.14	82.23
RFR	HH and HV	0.47	1.12	−0.22	78.59
	HH and VV	0.36	1.26	0.20	98.42
	HV and VV	0.79	0.77	0.20	70.60
(b) C-Band					
Method	**Polarizations**	**GAI [$m^2\,m^{-2}$]**		**V_m [$kg\,m^{-3}$]**	
		r	**RMSE**	**r**	**RMSE**
IO	VH and VV	0.59	1.27	0.16	87.80
LUT	VH and VV	0.54	1.22	0.21	81.15
RFR	VH and VV	0.65	0.98	0.29	69.34

5. Discussion

The sensitivity assessment of the L-band data, based on a regression analysis and simulations of the backscatter of the maize crop by forward modeling with the WCM, demonstrated the sensitivity of the L-band backscattering measurements to variations in the GAI in those crops. However, it also revealed the significantly lower sensitivity of the SAR measurements to the volumetric surface soil moisture under the canopy, possibly due to drought conditions, which is also apparent in the estimation results obtained from both retrieval methods, i.e., the algebraic inversion of the WCM and the joint estimation of both variables from radar backscatter measurements in two distinct polarizations.

The algebraic inversion of the WCM, the results of which are reported in Section 4.2, consists of finding one of the two variables of interest using the other as well as backscattering measurements in a single polarization and the incidence angle of the SAR beam. This method for either GAI or soil moisture retrieval provided more accurate results with SAR backscatter measurements in L-band rather than in C-band, especially for the GAI retrieval. Furthermore, for this purpose, the vertical co-polarization, VV, in L-band was the most adequate, but only slightly better than HV. For the estimation of the soil moisture under the canopy, on the other hand, while accuracies were low for all frequency bands and polarizations, the cross-polarization in L-band yielded the best results, while the horizontal co-polarization, HH, in L-band did not provide satisfactory results for either variable, as the sensitivity assessment prefigured. These findings are in agreement with the study of Tronquo et al. [63], who also exploited the BELSAR data set and reported that the most accurate soil moisture retrieval results over bare soils were found for VH and VV polarization. As for the C-band, finally, the cross-polarization, VH, provided more accurate estimates of both GAI and surface soil moisture than VV.

The simultaneous retrieval method, the results of which are reported in Section 4.3, dispensed with the need for ancillary data altogether and allowed the joint estimation of the two variables of interest simultaneously from dual-polarized SAR measurements and their incidence angle alone. Accurate GAI estimates were obtained with a strategy consisting of training a random forest regressor with data simulated by a pair WCMs

fitted on dual-polarized radar data. However, as with the first method, the accuracy of the surface soil moisture estimates obtained did not prove adequate enough for its monitoring, unlike the GAI estimates. The best accuracies for GAI retrieval with this method were obtained with L-band data in HV and VV polarizations, and the estimates derived from the C-band data from Sentinel-1 were not as good as those obtained from the L-band data from BELSAR. This second method did not provide GAI estimates as accurate as the previous one with the L-band data, though they were still fairly similar. It was the opposite for the C-band data. The similarity between the results of the first and second methods, as well as their accuracy, suggest that, under the specific conditions of the BELSAR campaign, knowledge of the volumetric surface soil moisture does not provide any improvement in accuracy for the estimation of the GAI of maize crops using the WCM with dual-polarized radar data.

The results show that the WCM is a simple and straightforward model to implement and operate which already works well with a limited amount of training data [64], although its calibration and estimation capabilities are very-dependent on them [35] and possibly quite inconsistent through time and space [17]. Its calibration procedure has proven to be robust and very independent of the choice of initial model parameters values. Moreover, it can be used with sufficient accuracy for the monitoring of maize crops, through their GAI, with ancillary information on surface soil moisture or only with radar data provided that two polarization channels are available.

In view of the results reported for its retrieval, monitoring the surface soil moisture under the canopy in maize fields is not possible with the WCM described in Section 3.1.1. Several hypotheses can explain the relative insensitivity of this model to soil moisture variations. The model for the soil contribution to the total backscatter suggested by Ulaby et al. [55], which depends linearly on volumetric surface soil moisture, might not be valid for the soil moisture conditions encountered, i.e., very dry soils and a very narrow range of surface moisture values due to an exceptionally dry season. The empirical Oh model [65] or the physically-based integral equation model (IEM) [66,67] and advanced integral equation model (AIEM) [68,69] could be used as an alternative to it. These models require an accurate description of the surface roughness, however, and its parameterization from field measurements is known to be problematic. This issue was addressed by Tronquo et al. [63], who proposed a method based on effective roughness modeling, whereby roughness parameters are calibrated based on backscatter observations, which can then be used for soil moisture retrieval. This approach could be implemented in the WCM framework in order to better reflect the actual soil contribution to the total backscatter. Another hypothesis explaining the insensitivity of the model to soil moisture invokes the attenuation of the signal by the already well-developed canopy as early as the second acquisition, on 21 June (F2), although it seems less likely in view of the penetration ability of the L-band [19]. The preponderance of double-bounce phenomena in the canopy that are not taken into account by the WCM could also explain the poor sensitivity of the model. Or finally, a combination of these different factors could be the cause of the inaccuracy of the results.

The accuracy of the GAI estimates obtained with the algebraic inversion of the WCM and the simultaneous estimation of the two variables is encouraging. As expected for high biomass crops, the L-band performs significantly better than the C-band in this respect. Only the HH polarization does not yield the same satisfactory results for the GAI retrieval. This might be due to an effect of the orientation of the maize rows relative to the SAR signal beam, which is much greater in HH than in HV or VV [50,70]. The results are otherwise getting close to, though remaining less accurate than, those that can be expected from remote sensing methods exploiting optical data; e.g., [5,71,72]. The use of radar-only data, however, has a significant advantage over them in the presence of cloud cover, which is frequent during the growing season, and especially at its end, in the area of interest. The GAI map in Figure 15 is an example of the relevance of such techniques. It reveals that harvesting has only begun in the northern part of the field, while the rest of the field is still vegetated, at a time when cloud cover is almost persistent.

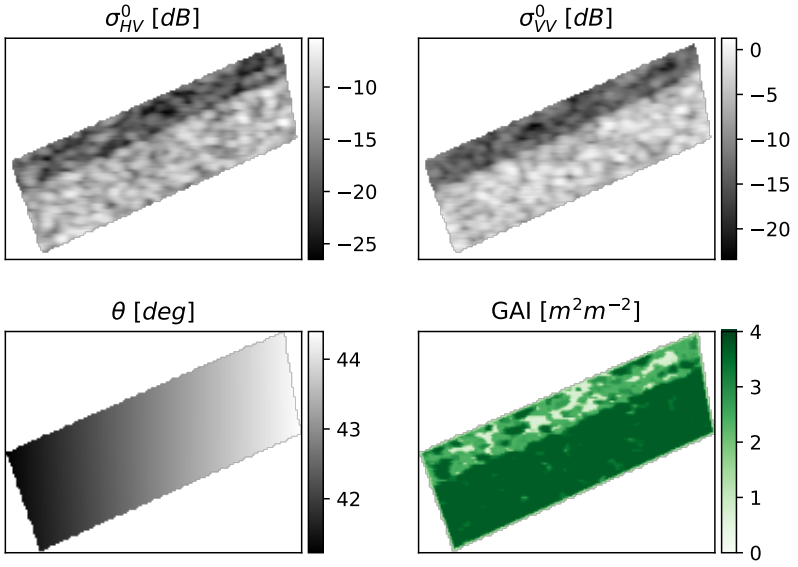

Figure 15. GAI map of a maize field, in which in-situ data were collected, produced using a RFR trained with L-band backscattering coefficients σ^0 in HV and VV polarizations acquired on 26 August (F4). To reduce speckle, a 5×5 boxcar filter was applied on the SAR images prior to GAI retrieval.

6. Conclusions

The WCM was used in this study for the simultaneous estimation of the GAI of maize crops and the surface soil moisture under their canopy from dual-polarized SAR data in C- and L-band. Accurate GAI estimates were obtained using a random forest regressor to invert a pair of WCMs calibrated with SAR data in cross-polarization and vertical co-polarization in both L- and C-band, with correlation coefficients of 0.79 and 0.65 and RMSEs of $0.77\,m^2\,m^{-2}$ and $0.98\,m^2\,m^{-2}$, respectively. However, the method was shown to be inadequate for soil moisture retrieval in the drought conditions of the field campaign.

These very encouraging results indicate that GAI retrieval in maize crops using only dual-polarized radar data could successfully substitute for estimates derived from optical data when these are not available, such as in the case of persistent cloud cover. Furthermore, the effectiveness of multi-polarized L-band data for GAI monitoring reported in this study highlights the relevance for agriculture of the further development and exploitation of spaceborne L-band SAR with a high revisit time. The upcoming launch of NISAR, ALOS-4, and Tandem-L, with their L-band, high temporal resolution, and systematic acquisition mode, will allow to extend and scale up the results of this study using a larger set of L-band SAR acquisitions and provide a valuable addition to the C- and X-band sensors already in orbit, which opens up exciting prospects for agricultural applications.

Author Contributions: Conceptualization, J.B. and P.D.; methodology, J.B. and P.D.; software, J.B.; validation, J.B. and E.T.; formal analysis, J.B.; investigation, J.B., E.T. and A.O.; resources, P.D.; data curation, J.B., E.T. and A.O.; writing—original draft preparation, J.B.; writing—review and editing, J.B., E.T., A.O., X.N., N.E.C.V. and P.D.; visualization, J.B.; supervision, P.D.; project administration, P.D.; funding acquisition, N.E.C.V. and P.D. All authors have read and agreed to the published version of the manuscript.

Funding: This research was conducted in the framework of the BELSAR-Science project jointly funded by the STEREO III program of the Belgian Federal Science Policy Office (BELSPO) under contract SR/00/371 and the PRODEX program of the European Space Agency (ESA) under contract 4000130658.

Data Availability Statement: Restrictions apply to the availability of the data presented in this study. The European Space Agency (ESA) will make the data available after a certain period of time.

Acknowledgments: The authors would like to thank the BELSAR-Campaign team for the collection of the joint airborne SAR and in-situ data sets used in this work, as well as Leila Guerriero from Tor Vergata University of Rome, Nazzareno Pierdicca from Sapienza University of Rome, and Hugh Griffiths from University College London, for participating in their scientific exploitation.

Conflicts of Interest: The authors declare no conflict of interest.

References

1. Delegido, J.; Verrelst, J.; Rivera, J.P.; Ruiz-Verdú, A.; Moreno, J. Brown and green LAI mapping through spectral indices. *Int. J. Appl. Earth Obs. Geoinf.* **2015**, *35*, 350–358. [CrossRef]
2. Duveiller, G.; Baret, F.; Defourny, P. Remotely sensed green area index for winter wheat crop monitoring: 10-Year assessment at regional scale over a fragmented landscape. *Agric. For. Meteorol.* **2012**, *166*, 156–168. [CrossRef]
3. Duveiller, G.; Weiss, M.; Baret, F.; Defourny, P. Retrieving wheat Green Area Index during the growing season from optical time series measurements based on neural network radiative transfer inversion. *Remote Sens. Environ.* **2011**, *115*, 887–896. [CrossRef]
4. Amin, E.; Verrelst, J.; Rivera-Caicedo, J.P.; Pipia, L.; Ruiz-Verdú, A.; Moreno, J. Prototyping Sentinel-2 green LAI and brown LAI products for cropland monitoring. *Remote Sens. Environ.* **2021**, *255*, 112168. [CrossRef]
5. Delloye, C.; Weiss, M.; Defourny, P. Retrieval of the canopy chlorophyll content from Sentinel-2 spectral bands to estimate nitrogen uptake in intensive winter wheat cropping systems. *Remote Sens. Environ.* **2018**, *216*, 245–261. [CrossRef]
6. Clevers, J.G.; Kooistra, L.; Van den Brande, M.M. Using Sentinel-2 data for retrieving LAI and leaf and canopy chlorophyll content of a potato crop. *Remote Sens.* **2017**, *9*, 405. [CrossRef]
7. Verrelst, J.; Rivera, J.P.; Veroustraete, F.; Muñoz-Marí, J.; Clevers, J.G.; Camps-Valls, G.; Moreno, J. Experimental Sentinel-2 LAI estimation using parametric, non-parametric and physical retrieval methods—A comparison. *ISPRS J. Photogramm. Remote Sens.* **2015**, *108*, 260–272. [CrossRef]
8. Verstraeten, W.W.; Veroustraete, F.; van der Sande, C.J.; Grootaers, I.; Feyen, J. Soil moisture retrieval using thermal inertia, determined with visible and thermal spaceborne data, validated for European forests. *Remote Sens. Environ.* **2006**, *101*, 299–314. [CrossRef]
9. Van doninck, J.; Peters, J.; De Baets, B.; De Clercq, E.M.; Ducheyne, E.; Verhoest, N.E. The potential of multitemporal Aqua and Terra MODIS apparent thermal inertia as a soil moisture indicator. *Int. J. Appl. Earth Obs. Geoinf.* **2011**, *13*, 934–941. [CrossRef]
10. Qin, J.; Yang, K.; Lu, N.; Chen, Y.; Zhao, L.; Han, M. Spatial upscaling of in-situ soil moisture measurements based on MODIS-derived apparent thermal inertia. *Remote Sens. Environ.* **2013**, *138*, 1–9. [CrossRef]
11. Babaeian, E.; Sadeghi, M.; Franz, T.E.; Jones, S.; Tuller, M. Mapping soil moisture with the OPtical TRApezoid Model (OPTRAM) based on long-term MODIS observations. *Remote Sens. Environ.* **2018**, *211*, 425–440. [CrossRef]
12. Rahimzadeh-Bajgiran, P.; Berg, A.A.; Champagne, C.; Omasa, K. Estimation of soil moisture using optical/thermal infrared remote sensing in the Canadian Prairies. *ISPRS J. Photogramm. Remote Sens.* **2013**, *83*, 94–103. [CrossRef]
13. Wang, K.; Franklin, S.E.; Guo, X.; He, Y.; McDermid, G.J. Problems in remote sensing of landscapes and habitats. *Prog. Phys. Geogr.* **2009**, *33*, 747–768. [CrossRef]
14. Defourny, P. Land cover mapping and monitoring. In *Handbook on Remote Sensing for Agricultural Statistics*; Food and Agriculture Organization of the United Nations (FAO): Rome, Italy, 2017; pp. 21–58. [CrossRef]
15. Jiao, X.; McNairn, H.; Shang, J.; Liu, J. The sensitivity of multi-frequency (X, C and L-band) radar backscatter signatures to bio-physical variables (LAI) over corn and soybean fields. In Proceedings of the ISPRS TC VII Symposium—100 Years ISPRS, Vienna, Austria, 5–7 July 2010; pp. 317–325.
16. Jiao, X.; McNairn, H.; Shang, J.; Pattey, E.; Liu, J.; Champagne, C. The sensitivity of RADARSAT-2 polarimetric SAR data to corn and soybean leaf area index. *Can. J. Remote Sens.* **2011**, *37*, 69–81. [CrossRef]
17. Beriaux, E.; Lucau-Danila, C.; Auquiere, E.; Defourny, P. Multiyear independent validation of the water cloud model for retrieving maize leaf area index from SAR time series. *Int. J. Remote Sens.* **2013**, *34*, 4156–4181. [CrossRef]
18. Ulaby, F.T.; Moore, R.K.; Fung, A.K. *Microwave Remote Sensing: From Theory to Applications*; Artech House: Norwood, MA, USA, 1986; Volume 3.
19. El Hajj, M.; Baghdadi, N.; Bazzi, H.; Zribi, M. Penetration analysis of SAR signals in the C and L bands for wheat, maize, and grasslands. *Remote Sens.* **2018**, *11*, 31. [CrossRef]
20. Blaes, X.; Defourny, P.; Wegmuller, U.; Della Vecchia, A.; Guerriero, L.; Ferrazzoli, P. C-band polarimetric indexes for maize monitoring based on a validated radiative transfer model. *IEEE Trans. Geosci. Remote Sens.* **2006**, *44*, 791–800. [CrossRef]
21. Veloso, A.; Mermoz, S.; Bouvet, A.; Le Toan, T.; Planells, M.; Dejoux, J.F.; Ceschia, E. Understanding the temporal behavior of crops using Sentinel-1 and Sentinel-2-like data for agricultural applications. *Remote Sens. Environ.* **2017**, *199*, 415–426. [CrossRef]
22. Vreugdenhil, M.; Wagner, W.; Bauer-Marschallinger, B.; Pfeil, I.; Teubner, I.; Rüdiger, C.; Strauss, P. Sensitivity of Sentinel-1 backscatter to vegetation dynamics: An Austrian case study. *Remote Sens.* **2018**, *10*, 1396. [CrossRef]
23. Khabbazan, S.; Vermunt, P.; Steele-Dunne, S.; Ratering Arntz, L.; Marinetti, C.; van der Valk, D.; Iannini, L.; Molijn, R.; Westerdijk, K.; van der Sande, C. Crop monitoring using Sentinel-1 data: A case study from The Netherlands. *Remote Sens.* **2019**, *11*, 1887. [CrossRef]

24. Yang, G.; Shi, Y.; Zhao, C.; Wang, J. Estimation of soil moisture from multi-polarized SAR data over wheat coverage areas. In Proceedings of the 2012 First International Conference on Agro-Geoinformatics (Agro-Geoinformatics), Shanghai, China, 2–4 August 2012; pp. 1–5. [CrossRef]
25. Gherboudj, I.; Magagi, R.; Berg, A.A.; Toth, B. Soil moisture retrieval over agricultural fields from multi-polarized and multi-angular RADARSAT-2 SAR data. *Remote Sens. Environ.* **2011**, *115*, 33–43. [CrossRef]
26. Bhogapurapu, N.; Dey, S.; Mandal, D.; Bhattacharya, A.; Karthikeyan, L.; McNairn, H.; Rao, Y. Soil moisture retrieval over croplands using dual-pol L-band GRD SAR data. *Remote Sens. Environ.* **2022**, *271*, 112900. [CrossRef]
27. Pampaloni, P.; Paloscia, S. Microwave emission and plant water content: A comparison between field measurements and theory. *IEEE Trans. Geosci. Remote Sens.* **1986**, *GE-24*, 900–905. [CrossRef]
28. Karam, M.A.; Fung, A.K.; Lang, R.H.; Chauhan, N.S. A microwave scattering model for layered vegetation. *IEEE Trans. Geosci. Remote Sens.* **1992**, *30*, 767–784. [CrossRef]
29. Toure, A.; Thomson, K.P.; Edwards, G.; Brown, R.J.; Brisco, B.G. Adaptation of the MIMICS backscattering model to the agricultural context-wheat and canola at L and C bands. *IEEE Trans. Geosci. Remote Sens.* **1994**, *32*, 47–61. [CrossRef]
30. Ferrazzoli, P.; Wigneron, J.P.; Guerriero, L.; Chanzy, A. Multifrequency emission of wheat: Modeling and applications. *IEEE Trans. Geosci. Remote Sens.* **2000**, *38*, 2598–2607. [CrossRef]
31. Macelloni, G.; Paloscia, S.; Pampaloni, P.; Marliani, F.; Gai, M. The relationship between the backscattering coefficient and the biomass of narrow and broad leaf crops. *IEEE Trans. Geosci. Remote Sens.* **2001**, *39*, 873–884. [CrossRef]
32. Della Vecchia, A.; Ferrazzoli, P.; Guerriero, L.; Blaes, X.; Defourny, P.; Dente, L.; Mattia, F.; Satalino, G.; Strozzi, T.; Wegmuller, U. Influence of geometrical factors on crop backscattering at C-band. *IEEE Trans. Geosci. Remote Sens.* **2006**, *44*, 778–790. [CrossRef]
33. Konings, A.G.; Piles, M.; Das, N.; Entekhabi, D. L-band vegetation optical depth and effective scattering albedo estimation from SMAP. *Remote Sens. Environ.* **2017**, *198*, 460–470. [CrossRef]
34. Attema, E.; Ulaby, F.T. Vegetation modeled as a water cloud. *Radio Sci.* **1978**, *13*, 357–364. [CrossRef]
35. Bériaux, E.; Waldner, F.; Collienne, F.; Bogaert, P.; Defourny, P. Maize leaf area index retrieval from synthetic quad pol SAR time series using the water cloud model. *Remote Sens.* **2015**, *7*, 16204–16225. [CrossRef]
36. Chauhan, S.; Srivastava, H.S.; Patel, P. Wheat crop biophysical parameters retrieval using hybrid-polarized RISAT-1 SAR data. *Remote Sens. Environ.* **2018**, *216*, 28–43. [CrossRef]
37. Park, S.E.; Jung, Y.T.; Cho, J.H.; Moon, H.; Han, S.h. Theoretical evaluation of water cloud model vegetation parameters. *Remote Sens.* **2019**, *11*, 894. [CrossRef]
38. Lievens, H.; Verhoest, N.E. On the retrieval of soil moisture in wheat fields from L-band SAR based on water cloud modeling, the IEM, and effective roughness parameters. *IEEE Geosci. Remote Sens. Lett.* **2011**, *8*, 740–744. [CrossRef]
39. Liu, C.; Shi, J. Estimation of vegetation parameters of water cloud model for global soil moisture retrieval using time-series L-band Aquarius observations. *IEEE J. Sel. Top. Appl. Earth Obs. Remote Sens.* **2016**, *9*, 5621–5633. [CrossRef]
40. Baghdadi, N.; El Hajj, M.; Zribi, M.; Bousbih, S. Calibration of the water cloud model at C-band for winter crop fields and grasslands. *Remote Sens.* **2017**, *9*, 969. [CrossRef]
41. Wang, Z.; Zhao, T.; Qiu, J.; Zhao, X.; Li, R.; Wang, S. Microwave-based vegetation descriptors in the parameterization of water cloud model at L-band for soil moisture retrieval over croplands. *Giscience Remote Sens.* **2021**, *58*, 48–67. [CrossRef]
42. Rains, D.; Lievens, H.; De Lannoy, G.J.; McCabe, M.F.; de Jeu, R.A.; Miralles, D.G. Sentinel-1 Backscatter Assimilation Using Support Vector Regression or the Water Cloud Model at European Soil Moisture Sites. *IEEE Geosci. Remote Sens. Lett.* **2021**, *19*, 1–5. [CrossRef]
43. Zribi, M.; Muddu, S.; Bousbih, S.; Al Bitar, A.; Tomer, S.K.; Baghdadi, N.; Bandyopadhyay, S. Analysis of L-band SAR data for soil moisture estimations over agricultural areas in the tropics. *Remote Sens.* **2019**, *11*, 1122. [CrossRef]
44. Bériaux, E.; Lambot, S.; Defourny, P. Estimating surface-soil moisture for retrieving maize leaf-area index from SAR data. *Can. J. Remote Sens.* **2011**, *37*, 136–150. [CrossRef]
45. Mandal, D.; Hosseini, M.; McNairn, H.; Kumar, V.; Bhattacharya, A.; Rao, Y.; Mitchell, S.; Robertson, L.D.; Davidson, A.; Dabrowska-Zielinska, K. An investigation of inversion methodologies to retrieve the leaf area index of corn from C-band SAR data. *Int. J. Appl. Earth Obs. Geoinf.* **2019**, *82*, 101893. [CrossRef]
46. Hosseini, M.; McNairn, H. Using multi-polarization C-and L-band synthetic aperture radar to estimate biomass and soil moisture of wheat fields. *Int. J. Appl. Earth Obs. Geoinf.* **2017**, *58*, 50–64. [CrossRef]
47. Hosseini, M.; McNairn, H.; Merzouki, A.; Pacheco, A. Estimation of Leaf Area Index (LAI) in corn and soybeans using multi-polarization C-and L-band radar data. *Remote Sens. Environ.* **2015**, *170*, 77–89. [CrossRef]
48. de Macedo, K.A.C.; Placidi, S.; Meta, A. Bistatic and Monostatic inSAR Results with the MetaSensing Airborne SAR System. In Proceedings of the 2019 6th Asia-Pacific Conference on Synthetic Aperture Radar (APSAR), Xiamen, China, 26–29 November 2019; pp. 1–5. [CrossRef]
49. Fore, A.G.; Chapman, B.D.; Hawkins, B.P.; Hensley, S.; Jones, C.E.; Michel, T.R.; Muellerschoen, R.J. UAVSAR polarimetric calibration. *IEEE Trans. Geosci. Remote Sens.* **2015**, *53*, 3481–3491. [CrossRef]
50. Bouchat, J.; Tronquo, E.; Orban, A.; Verhoest, N.E.; Defourny, P. Assessing the Potential of Fully Polarimetric Mono-and Bistatic SAR Acquisitions in L-band for Crop and Soil Monitoring. *IEEE J. Sel. Top. Appl. Earth Obs. Remote Sens.* **2022**, *15*, 3168–3178. [CrossRef]
51. SNAP—ESA Sentinel Application Platform v8.0.0. 2020. Available online: https://step.esa.int/ (accessed on 10 March 2022).

52. Eros, U. *USGS EROS Archive—Digital Elevation—Shuttle Radar Topography Mission (SRTM) 1 Arc-Second Global*; US Geological 766 Survey: Reston, VA, USA, 2015. [CrossRef]
53. Meier, U. *Growth Stages of Mono- and Dicotyledonous Plants*; Blackwell Wissenschafts-Verlag: Berlin, Germany, 1997.
54. Prevot, L.; Champion, I.; Guyot, G. Estimating surface soil moisture and leaf area index of a wheat canopy using a dual-frequency (C and X bands) scatterometer. *Remote Sens. Environ.* **1993**, *46*, 331–339. [CrossRef]
55. Ulaby, F.T.; Batlivala, P.P.; Dobson, M.C. Microwave backscatter dependence on surface roughness, soil moisture, and soil texture: Part I-bare soil. *IEEE Trans. Geosci. Electron.* **1978**, *16*, 286–295. [CrossRef]
56. Wales, D.J.; Doye, J.P. Global optimization by basin-hopping and the lowest energy structures of Lennard-Jones clusters containing up to 110 atoms. *J. Phys. Chem. A* **1997**, *101*, 5111–5116. [CrossRef]
57. Nash, S.G. Newton-type minimization via the Lanczos method. *SIAM J. Numer. Anal.* **1984**, *21*, 770–788. [CrossRef]
58. Kelley, C.T. *Iterative Methods for Optimization*; SIAM: Philadelphia, PA, USA, 1999. [CrossRef]
59. Breiman, L. Random forests. *Mach. Learn.* **2001**, *45*, 5–32. [CrossRef]
60. Moré, J.J. The Levenberg-Marquardt algorithm: Implementation and theory. In *Numerical Analysis*; Springer: Berlin/Heidelberg, Germany, 1978; pp. 105–116. [CrossRef]
61. Probst, P.; Wright, M.N.; Boulesteix, A.L. Hyperparameters and tuning strategies for random forest. *Wiley Interdiscip. Rev. Data Min. Knowl. Discov.* **2019**, *9*, e1301. [CrossRef]
62. Wiseman, G.; McNairn, H.; Homayouni, S.; Shang, J. RADARSAT-2 polarimetric SAR response to crop biomass for agricultural production monitoring. *IEEE J. Sel. Top. Appl. Earth Obs. Remote Sens.* **2014**, *7*, 4461–4471. [CrossRef]
63. Tronquo, E.; Lievens, H.; Bouchat, J.; Defourny, P.; Baghdadi, N.; Verhoest, N.E.C. Soil Moisture Retrieval Using Multistatic L-Band SAR and Effective Roughness Modeling. *Remote Sens.* **2022**, *14*, 1650. [CrossRef]
64. Hosseini, M.; McNairn, H.; Mitchell, S.; Robertson, L.D.; Davidson, A.; Ahmadian, N.; Bhattacharya, A.; Borg, E.; Conrad, C.; Dabrowska-Zielinska, K.; et al. A comparison between support vector machine and water cloud model for estimating crop leaf area index. *Remote Sens.* **2021**, *13*, 1348. [CrossRef]
65. Oh, Y.; Sarabandi, K.; Ulaby, F.T. An empirical model and an inversion technique for radar scattering from bare soil surfaces. *IEEE Trans. Geosci. Remote Sens.* **1992**, *30*, 370–381. [CrossRef]
66. Fung, A.K.; Li, Z.; Chen, K.S. Backscattering from a randomly rough dielectric surface. *IEEE Trans. Geosci. Remote Sens.* **1992**, *30*, 356–369. [CrossRef]
67. Fung, A.K. *Microwave Scattering and Emission Models and Their Applications*; Artech House: London, UK, 1994.
68. Chen, K.S.; Wu, T.D.; Tsang, L.; Li, Q.; Shi, J.; Fung, A.K. Emission of rough surfaces calculated by the integral equation method with comparison to three-dimensional moment method simulations. *IEEE Trans. Geosci. Remote Sens.* **2003**, *41*, 90–101. [CrossRef]
69. Wu, T.D.; Chen, K.S. A reappraisal of the validity of the IEM model for backscattering from rough surfaces. *IEEE Trans. Geosci. Remote Sens.* **2004**, *42*, 743–753. [CrossRef]
70. Bouchat, J.; Defourny, P. Effect of Row Orientation on Maize Green Area Index Retrieval from L-Band Synthetic Aperture Radar Imagery. In Proceedings of the 2021 IEEE International Geoscience and Remote Sensing Symposium IGARSS, Brussels, Belgium, 11–16 July 2021; pp. 6716–6719. [CrossRef]
71. Peng, X.; Han, W.; Ao, J.; Wang, Y. Assimilation of LAI Derived from UAV Multispectral Data into the SAFY Model to Estimate Maize Yield. *Remote Sens.* **2021**, *13*, 1094. [CrossRef]
72. Yu, L.; Shang, J.; Cheng, Z.; Gao, Z.; Wang, Z.; Tian, L.; Wang, D.; Che, T.; Jin, R.; Liu, J.; et al. Assessment of Cornfield LAI Retrieved from Multi-Source Satellite Data Using Continuous Field LAI Measurements Based on a Wireless Sensor Network. *Remote Sens.* **2020**, *12*, 3304. [CrossRef]